

# Supplementary Information: $\text{Cu}_2\text{SiSe}_3$ as a promising solar absorber: harnessing cation dissimilarity to avoid killer antisites

Adair Nicolson,<sup>†</sup> Seán R. Kavanagh,<sup>†,‡</sup> Christopher N. Savory,<sup>†</sup> Graeme W. Watson,<sup>¶</sup> and David O. Scanlon<sup>\*,†</sup>

<sup>†</sup>*Thomas Young Centre and Department of Chemistry, University College London, 20 Gordon Street, London WC1H 0AJ, U.K.*

<sup>‡</sup>*Thomas Young Centre and Department of Materials, Imperial College London, Exhibition Road, London SW7 2AZ, U.K.*

<sup>¶</sup>*School of Chemistry and CRANN, Trinity College Dublin, College Green, Dublin 2, Ireland*

E-mail: d.scanlon@ucl.ac.uk

## S1. Lattice Parameters

Table S1: Calculated lattice parameters for  $\text{Cu}_2\text{SiSe}_3$  using PBEsol and hybrid DFT (HSE06) with and without the inclusion of vdW dispersion interactions. Dispersion interactions are accounted for using the D3 correction with and without Becke-Johnson dampening. Percentage errors are with respect to experimental values.<sup>S1</sup>

	a	b	c
PBEsol	6.64 Å (-0.4 %)	11.65 Å (-1.3 %)	6.66 Å (0.4 %)
HSE06	6.70 Å (0.4 %)	11.84 Å (0.3 %)	6.67 Å (0.6 %)
HSE06+D3	6.62 Å (-0.7 %)	11.67 Å (-1.1 %)	6.58 Å (-0.8 %)
HSE06+D3(BJ)	6.60 Å (-1.0 %)	11.67 Å (-1.1 %)	6.57 Å (-0.9 %)

## S2. Electronic Structure

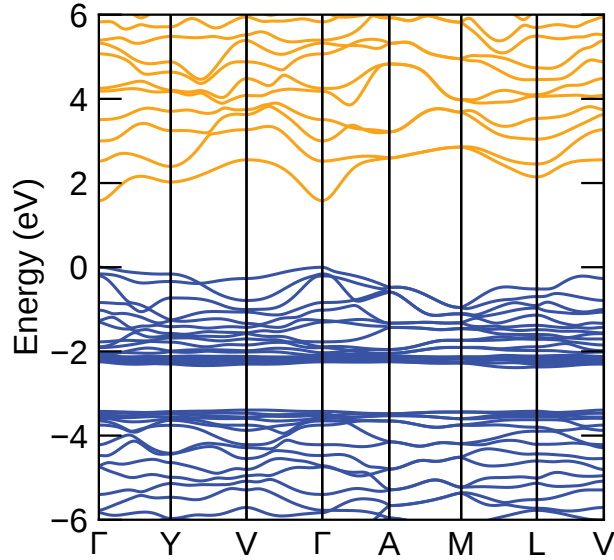


Figure S1: Electronic band structure of  $\text{Cu}_2\text{SiSe}_3$  calculated with  $\text{QSG}\hat{W}$ . The valence band maximum is set to 0 eV, with valence bands in blue and conduction bands in orange.

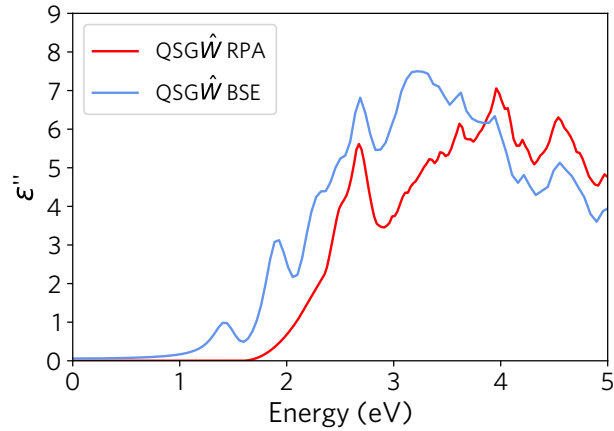


Figure S2: The z component of the imaginary dielectric spectrum of  $\text{Cu}_2\text{SiSe}_3$  calculated with  $\text{QSG}\hat{W}$  self-energy within the Random Phase approximation (RPA) and Bethe-Salpeter equation (BSE).

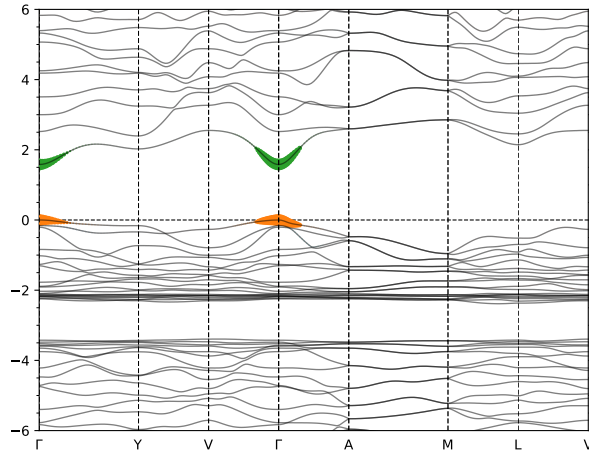


Figure S3: Electronic band structure of  $\text{Cu}_2\text{SiSe}_3$  calculated with  $\text{QSG}\hat{W}$ , with exciton wavefunction weights projected onto the corresponding bands. The valence band maximum is set to 0 eV.

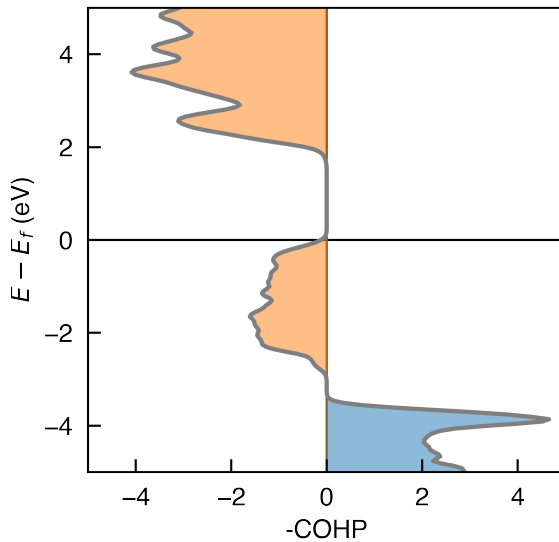


Figure S4: Cumulative Crystal Orbital Hamiltonian Population (COHP) analysis, which decomposes the density of states into bonding and anti-bonding orbital interactions.<sup>S2-S4</sup> Negative COHP values (blue) indicate bonding-type interactions and positive values (orange) indicate anti-bonding interactions.

### S3. Chemical potential space

To calculate the region of stability for  $\text{Cu}_2\text{SiSe}_3$ , the bordering competing phases were obtained from the Material Project.<sup>S5</sup> However, care must be taken due to the formation

energies predicted by the Material Projects (GGA/GGA+U) having a mean absolute error of 0.133 eV/atom.<sup>S6</sup> Furthermore, when looking at the predicted compositional phase diagram for Cu-Si-Se it can be seen that Cu<sub>2</sub>Se is found to lie 0.083 eV/atom above the hull, although it is found to be stable experimentally and is a commonly used precursor. Therefore, the formation energies of additional competing phases (found in the Inorganic Crystal Structure Database<sup>S7</sup>) were calculated using HSE06, rather than just the predicted bordering phases.

Calculating the formation energy of the competing phases using HSE06 predicts a much larger region of chemical stability, with the region no longer being bound only by Cu<sub>3</sub>Se<sub>2</sub>, SiSe<sub>2</sub> and Cu. Furthermore, using hybrid density functional theory (DFT), Cu<sub>2</sub>Se is found to be stable, lying on hull. The driving factor for this increase in stability is the lowering of the formation energy of Cu<sub>2</sub>SiSe<sub>3</sub>, when calculated using hybrid DFT, due to the lowering in energy of the Cu *d* states. To check that the increase in stability was not due to errors introduced in modeling selenium containing phases, through the exclusion of Van der Waals interactions, the formation energies were also determined using the HSE06+D3 functional. The formations energies of SiSe<sub>2</sub> and Cu<sub>3</sub>Se<sub>2</sub>, calculated with HSE06+D3, were found to be within 14 meV/atom and 3 meV/atom of those predicted by the Material Project using R2SCAN, which has been shown to reduce the error in predicted formation energies by up to a factor of 2.5.<sup>S8,S9</sup> However, using HSE06/HSE06+D3 we find the formation energy of Cu<sub>2</sub>SiSe<sub>3</sub> to lie 70/69 meV/atom lower in energy.

Table S2: The elemental chemical potentials at the intersections binding the chemical space for Cu<sub>2</sub>SiSe<sub>3</sub>. Intersection D and C correspond to Cu-rich conditions and G to Cu-poor.

	Cu (eV)	Si (eV)	Se (eV)
A	-0.08	-0.08	-0.76
B	-0.10	-1.10	-0.41
C	0.00	-0.72	-0.60
D	0.00	-0.39	-0.71
E	-0.29	-1.60	-0.11
F	-0.41	-1.71	0.00
G	-0.46	-1.59	0.00

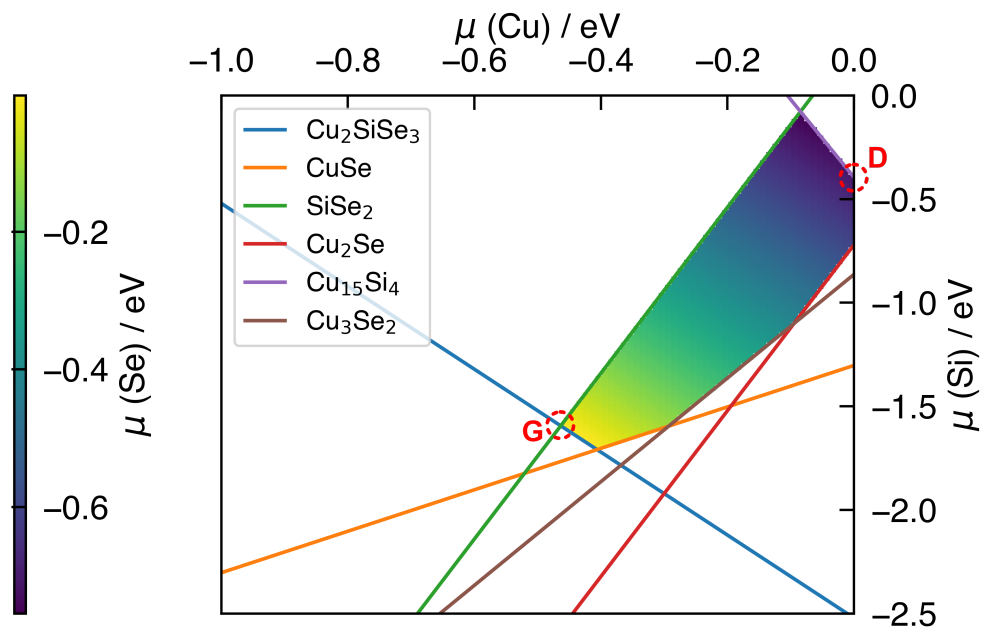


Figure S5: The chemical potential space of  $\text{Cu}_2\text{SiSe}_3$ . Intersection D corresponds to Cu-rich conditions and G to Cu-poor.

## S4. Defect Formation Energy Diagrams

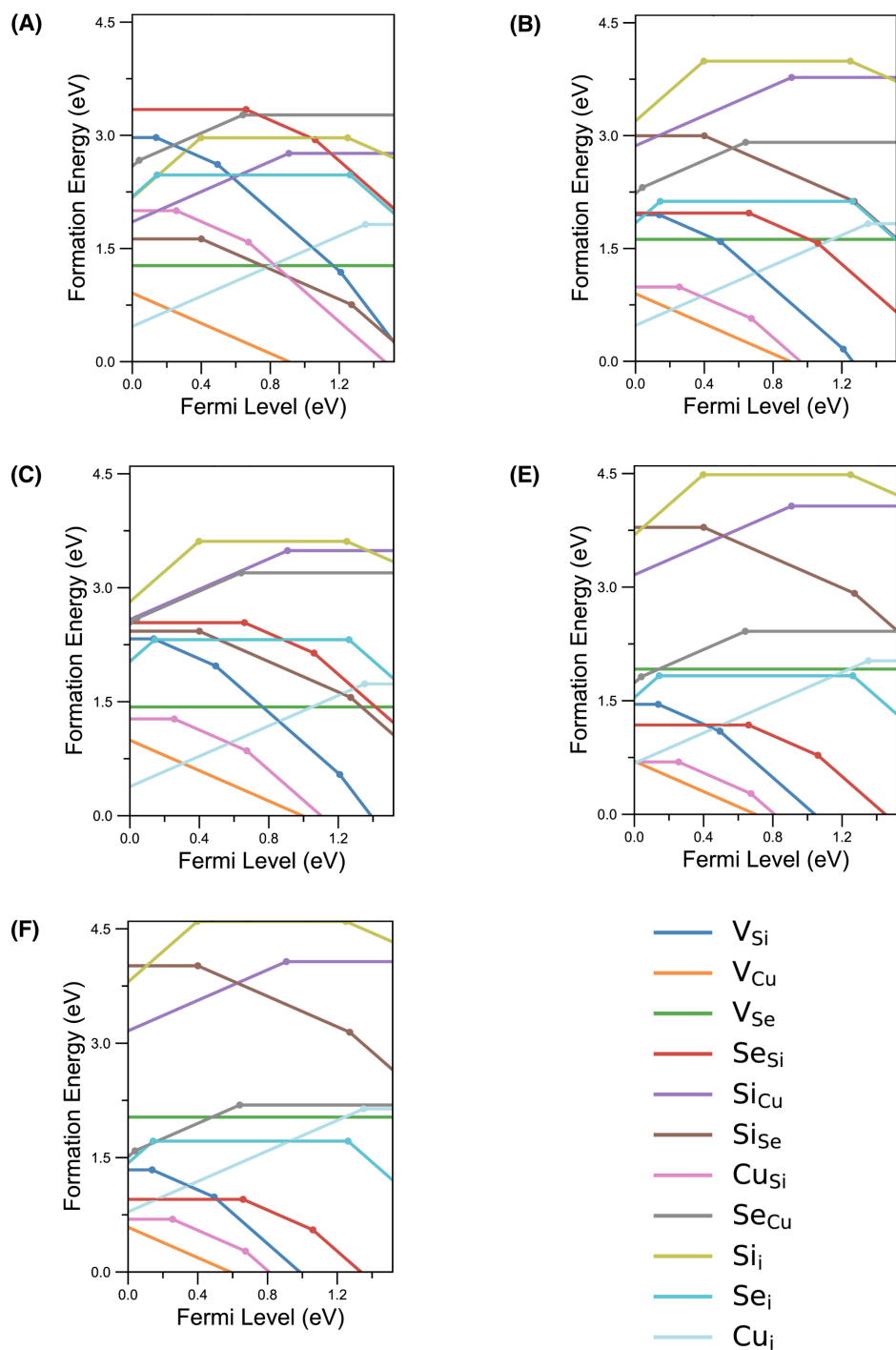


Figure S6: Formation energies as a function of Fermi level for the intrinsic defects in  $\text{Cu}_2\text{SiSe}_3$ . Labelling refers to the position on the chemical phase diagram, Table S3. For each defect species, only the lowest energy defect site has been plotted.

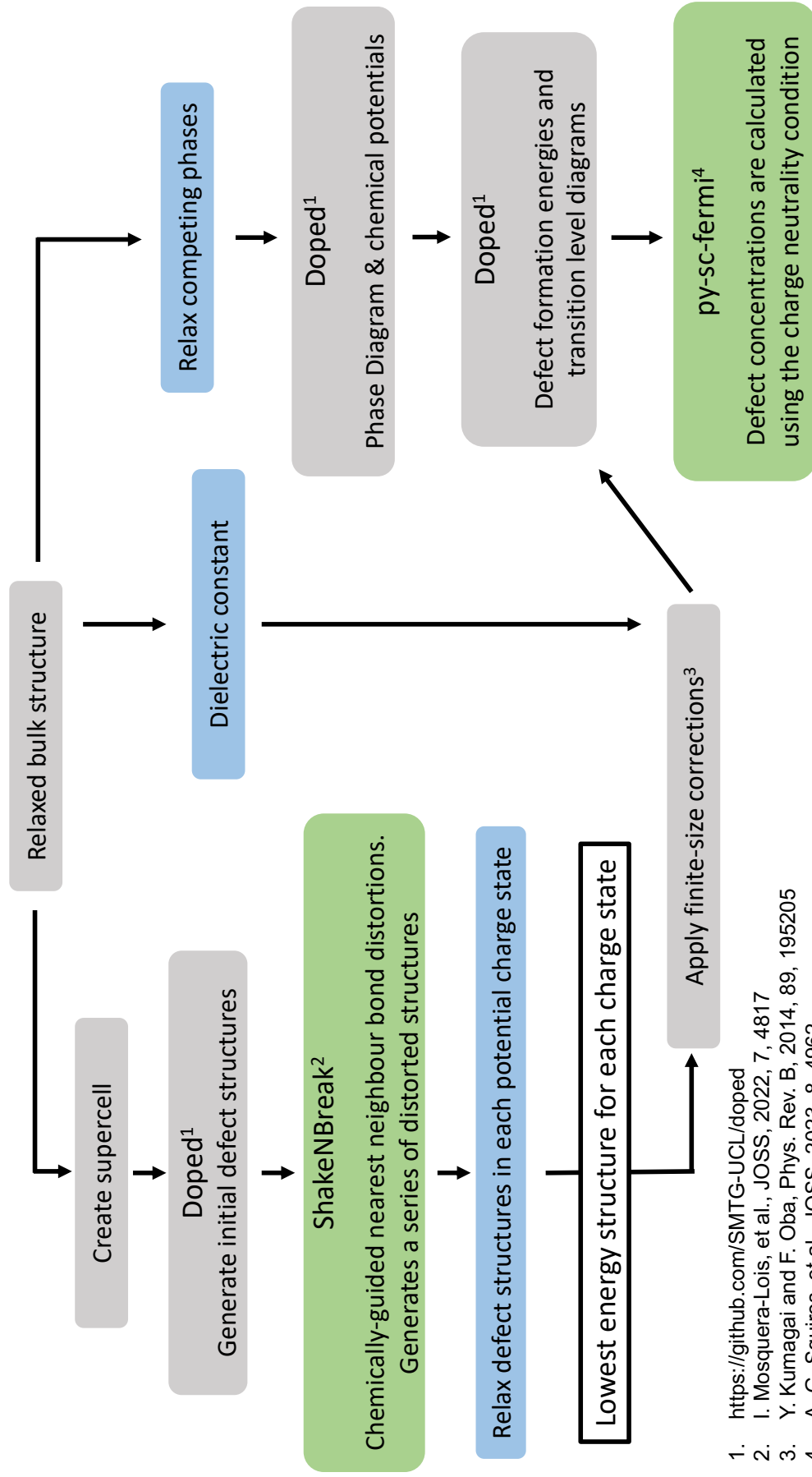


Figure S7: Defect calculation workflow.

1. <https://github.com/SMTG-UCL/doped>
2. I. Mosquera-Lois, et al., JOSS, 2022, 7, 4817
3. Y. Kumagai and F. Oba, Phys. Rev. B, 2014, 89, 195205
4. A. G. Squires, et al., JOSS, 2023, 8, 4962

Table S3: Number of defect types and charge states studied in this work

	Defect species	Sites	Charge states
Vacancy	$V_{\text{Cu}}$	2	-1,0
	$V_{\text{Si}}$	1	-4,-3,-2,-1,0
	$V_{\text{Se}}$	3	0,1,2
Antisite	$\text{Cu}_{\text{Si}}$	1	-4,-3,-2,-1,0
	$\text{Si}_{\text{Cu}}$	2	0,1,2,3
	$\text{Si}_{\text{Se}}$	3	-2,-1,0
	$\text{Se}_{\text{Cu}}$	2	0,1,2,3,4,5
	$\text{Se}_{\text{Si}}$	1	-4,-3,-2,-1,0,1,2,3,4
Interstitial	$\text{Cu}_i$	17	0,1
	$\text{Si}_i$	17	-4,-3,-2,-1,0,1,2,3,4
	$\text{Se}_i$	17	-2,-1,0,1,2,3,4,5,6

## S5. Copper Vacancy and Copper Antisites

A quantitative way to determine if a defect state is a perturbed host state (PSHS) is to use the screening method developed by Kumagai et al.,<sup>S10</sup> which defines a PHS as being a VBM-like state within 0.5 eV of the VBM (Figure S10b) and having an orbital dissimilarity less than 0.4. They define orbital dissimilarity as,

$$\Delta_m = \sum_{e,i} |\phi_{vacancy}^{m,e,i} - \phi_{bulk}^{e,i}| \quad (\text{S1})$$

where  $\phi_{vacancy}^{e,i}$  is the sum of the projections on element  $e$  and orbital  $i$  ( $i = s, p, d, \text{or } f$ ) at the  $m$ th band in the supercell with the vacancy and  $\phi_{perfect}^{e,i}$  is that at the VBM in the perfect supercell. Using their metric, the neutral vacancy is found to be VBM-like with an orbital dissimilarity of 0.01. This indicated that in the case of  $V_{\text{Cu}}$ , the neutral defect state is actually a  $V_{\text{Cu}}^-$  plus a delocalized hole. This can be seen by visualizing the charge density of the neutral defect where the defect state is delocalized across the supercell and comparing to the bulk, Figure S8a and S9. To accurately calculate the energy of such a shallow acceptor level, a supercell of several thousand of atoms is required.<sup>S11</sup> Increasing the size of the supercell from 96 atoms to 160 atoms reduced the transition level from 0.16 eV above the VBM to 0.10 eV. For a PHS it is expected for the formation energy of the neutral vacancy to

be almost the same as the charge defect state when the Fermi level is at the VBM. Therefore, we have set the transition level for a  $V_{\text{Cu}}$  in  $\text{Cu}_2\text{SiSe}_3$  to 0 eV above the VBM.

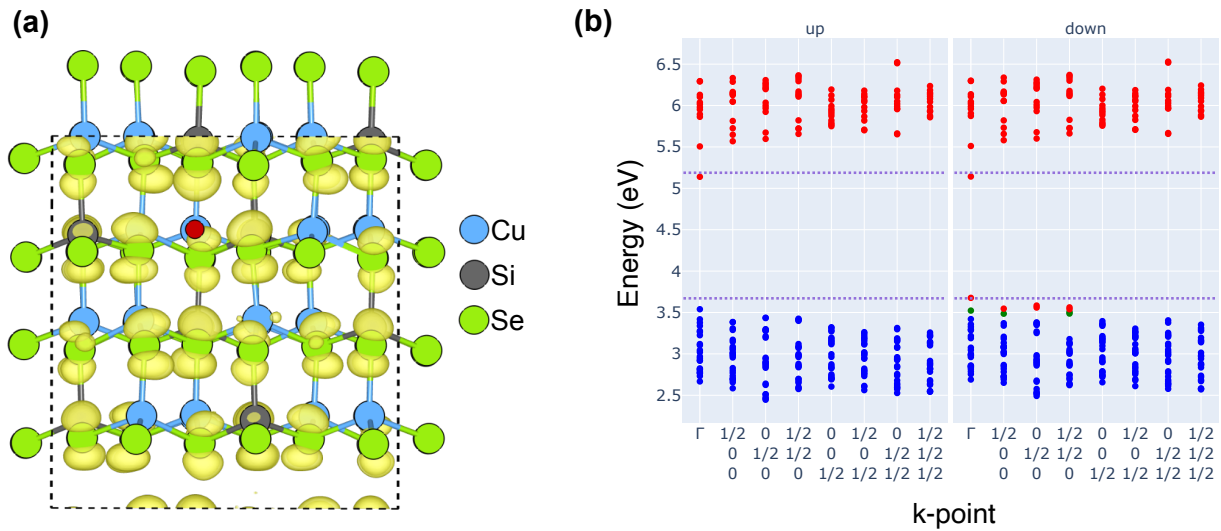


Figure S8: (a) Structure and spin down charge density of a neutral copper vacancy defect state at the VBM. Copper vacancy represented by the red circle. Isovalue set to  $1 \times 10^{-3} e/\text{\AA}^3$ . (b) Plot of the eigenvalues of a neutral copper vacancy defect state. Occupied levels are blue, unoccupied red, and partially occupied are colored green. The VBM and CBM of the pristine supercell are shown by the dashed line.

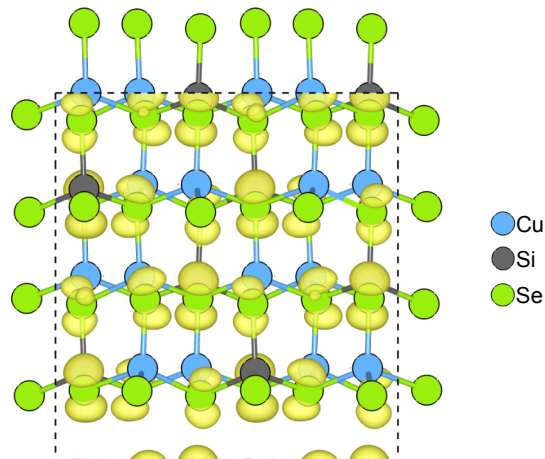


Figure S9: Charge density at the valence band in bulk  $\text{Cu}_2\text{SiSe}_3$ . Isovalue set to  $1 \times 10^{-3} e/\text{\AA}^3$ .

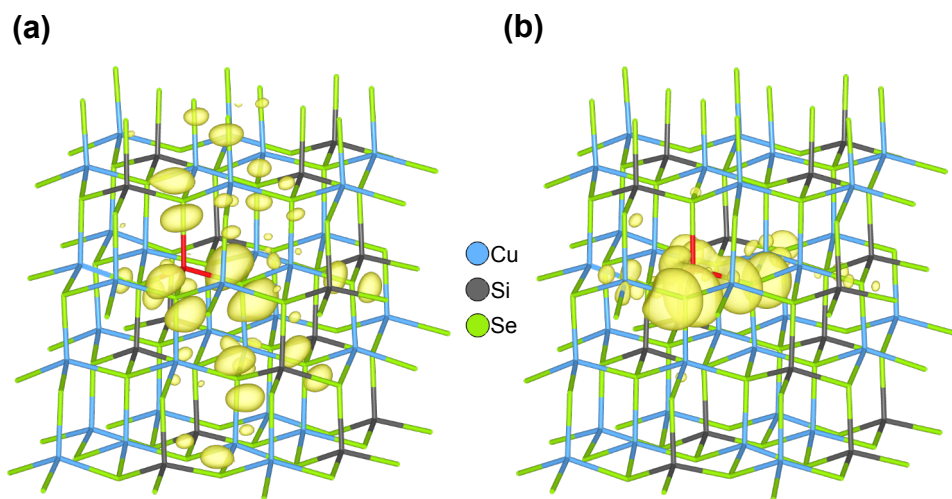


Figure S10: Structure and charge density ((a) spin up and (b) spin down) of a neutral copper on silicon antisite. The  $\text{Cu}_{\text{Si}}$  site is colored red. Isovalue set to  $6 \times 10^{-3} e/\text{\AA}^3$ .

## S6. Ground State Structure Searching

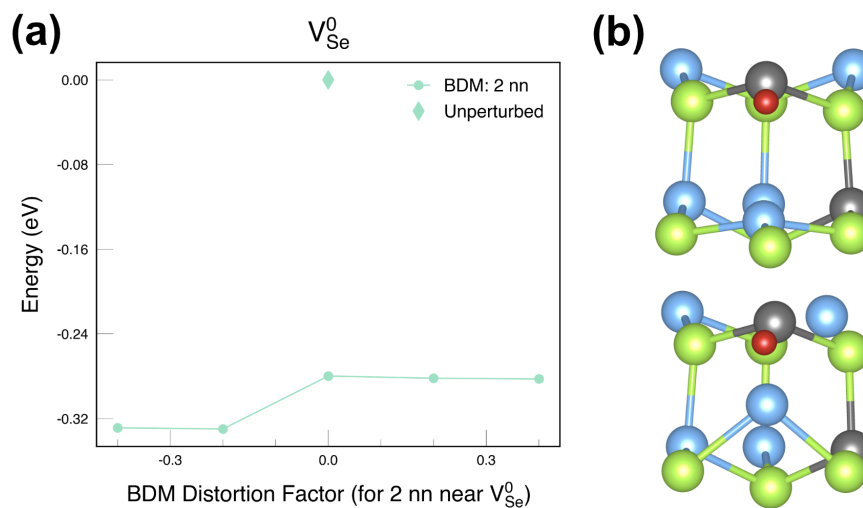


Figure S11: (a)  $V_{Se}^0$  bond distortion method (BDM) plot; nn refers to the number of nearest-neighbours distorted around the defect site. (b) Unperturbed defect structure (top) and energy lowering reconfiguration (bottom). Vacancy indicated by red circle. The lowest energy defect structure was also identified as the ground state structure for all charge states.

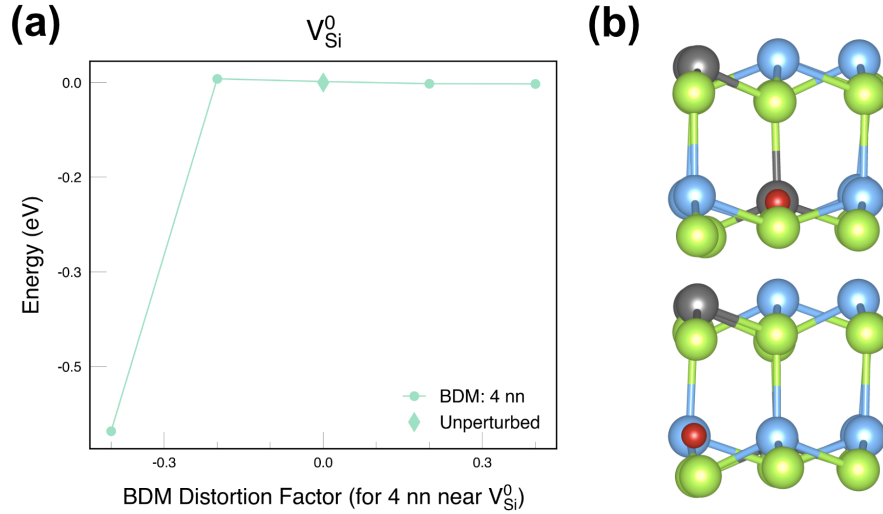


Figure S12: (a)  $V_{\text{Si}}^0$  bond distortion method (BDM) plot; nn refers to the number of nearest-neighbours distorted around the defect site. (b) Unperturbed defect structure (top) and energy lowering reconfiguration (bottom). Vacancy indicated by red circle. The lowest energy defect structure was also identified as the ground state structure for all charge states.

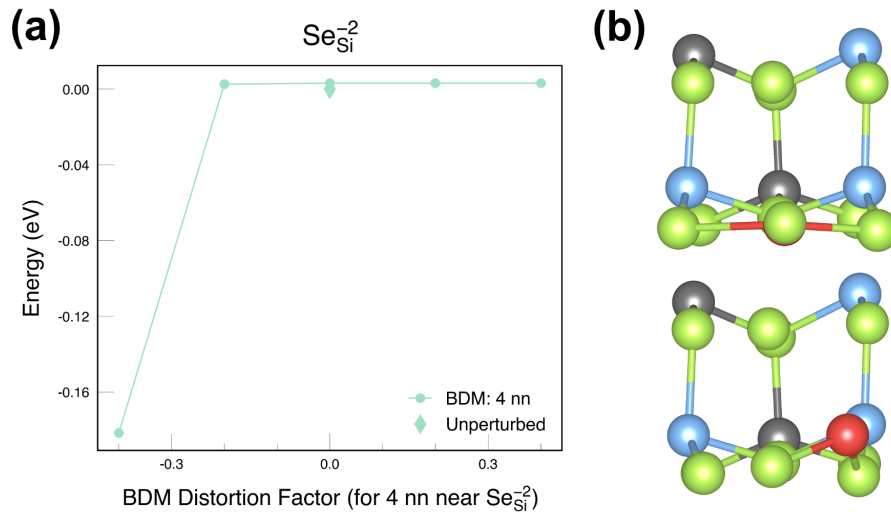


Figure S13: (a)  $\text{Se}_{\text{Si}}^{-2}$  bond distortion method (BDM) plot; nn refers to the number of nearest-neighbours distorted around the defect site. (b) Unperturbed defect structure (top) and energy lowering reconfiguration (bottom). Antisite colored red. The lowest energy defect structure was also identified as the ground state structure in the -1 charge state.

## References

- [S1] Chen, X.-a.; Wada, H.; Sato, A.; Nozaki, H. Synthesis, Structure, and Electronic Properties of  $\text{Cu}_2\text{SiQ}_3$  (Q=S, Se). *Journal of Alloys and Compounds* **1999**, *290*, 91–96.
- [S2] Deringer, V. L.; Tchougréeff, A. L.; Dronskowski, R. Crystal Orbital Hamilton Population (COHP) Analysis As Projected from Plane-Wave Basis Sets. *The Journal of Physical Chemistry A* **2011**, *115*, 5461–5466.
- [S3] Dronskowski, R.; Bloechl, P. E. Crystal Orbital Hamilton Populations (COHP): Energy-Resolved Visualization of Chemical Bonding in Solids Based on Density-Functional Calculations. *The Journal of Physical Chemistry* **1993**, *97*, 8617–8624.
- [S4] Nelson, R.; Ertural, C.; George, J.; Deringer, V. L.; Hautier, G.; Dronskowski, R. LOBSTER: Local Orbital Projections, Atomic Charges, and Chemical-Bonding Analysis from Projector-Augmented-Wave-Based Density-Functional Theory. *Journal of Computational Chemistry* **2020**, *41*, 1931–1940.
- [S5] Jain, A.; Ong, S. P.; Hautier, G.; Chen, W.; Richards, W. D.; Dacek, S.; Cholia, S.; Gunter, D.; Skinner, D.; Ceder, G.; Persson, K. A. Commentary: The Materials Project: A Materials Genome Approach to Accelerating Materials Innovation. *APL Materials* **2013**, *1*, 011002.
- [S6] Kirklin, S.; Saal, J. E.; Meredig, B.; Thompson, A.; Doak, J. W.; Aykol, M.; Rühl, S.; Wolverton, C. The Open Quantum Materials Database (OQMD): Assessing the Accuracy of DFT Formation Energies. *npj Computational Materials* **2015**, *1*, 1–15.
- [S7] Zagorac, D.; Müller, H.; Ruehl, S.; Zagorac, J.; Rehme, S. Recent Developments in the Inorganic Crystal Structure Database: Theoretical Crystal Structure Data and Related Features. *Journal of Applied Crystallography* **2019**, *52*, 918–925.

- [S8] Kothakonda, M.; Kaplan, A. D.; Isaacs, E. B.; Bartel, C. J.; Furness, J. W.; Ning, J.; Wolverton, C.; Perdew, J. P.; Sun, J. Testing the r2SCAN Density Functional for the Thermodynamic Stability of Solids with and without a van Der Waals Correction. *ACS Materials Au* **2022**,
- [S9] Furness, J. W.; Kaplan, A. D.; Ning, J.; Perdew, J. P.; Sun, J. Accurate and Numerically Efficient r2SCAN Meta-Generalized Gradient Approximation. *The Journal of Physical Chemistry Letters* **2020**, *11*, 8208–8215.
- [S10] Kumagai, Y.; Tsunoda, N.; Takahashi, A.; Oba, F. Insights into Oxygen Vacancies from High-Throughput First-Principles Calculations. *Physical Review Materials* **2021**, *5*, 123803.
- [S11] Zhang, G.; Canning, A.; Grønbech-Jensen, N.; Derenzo, S.; Wang, L.-W. Shallow Impurity Level Calculations in Semiconductors Using Ab Initio Methods. *Physical Review Letters* **2013**, *110*, 166404.